Composition-Tunable Formamidinium Lead Mixed Halide Perovskites via Solvent-Free Mechanochemical Synthesis: Decoding the Pb Environments Using Solid-State NMR Spectroscopy

*Abdelrahman M. Askar,[1,§] Abhoy Karmakar,[2,§] Guy M. Bernard,[2] Michelle Ha,[2] Victor V. Terskikh,[3] Benjamin D. Wiltshire,[1] Sahil Patel,[1] Jonathan Fleet,[1] Karthik Shankar,[1] and Vladimir K. Michaelis[2]**

1- Department of Electrical and Computer Engineering, University of Alberta, Edmonton, Alberta, Canada, T6G 1H9
2- Department of Chemistry, University of Alberta, Edmonton, Alberta, Canada, T6G 2G2
3- Department of Chemistry, University of Ottawa, Ottawa, Ontario, Canada, K1N 6N5

Mixed-halide lead perovskites are becoming of paramount interest in the optoelectronic and photovoltaic research fields, offering bandgap tunability, improved efficiency and enhanced stability compared to their single halide counterparts. Formamidinium-based mixed halide perovskites (FA-MHPs) are critical to obtaining optimum solar cell performance. Here, we report a solvent-free mechanochemical synthesis (MCS) method to prepare FA-MHPs, starting with their parent compounds ($FAPbX_3$; X = Cl, Br, I), achieving compositions not previously accessible through the solvent synthesis (SS) technique. By probing local Pb environments in MCS FA-MHPs using solid-state nuclear magnetic resonance spectroscopy, along with powder X-ray diffraction for long-range crystallinity and reflectance measurements to determine the optical bandgap, we show that MCS FA-MHPs form atomic-level solid-solutions between Cl/Br and Br/I MHPs. Our results pave the way for advanced methods in atomic-level structural understanding while offering a one-pot synthetic approach to prepare MHPs with superior control of stoichiometry.

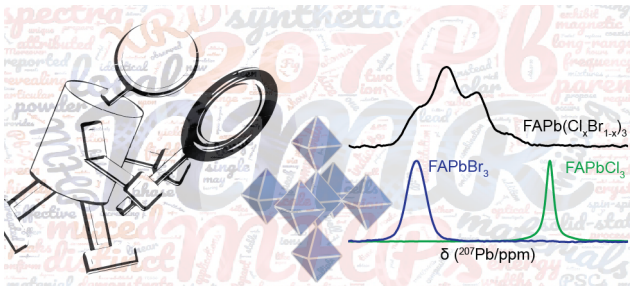

Organic-inorganic halide perovskites have emerged as promising and captivating candidates for next-generation low-cost and high-efficiency solar cells due to their excellent optoelectronic properties[1] and solution processability.[2] With photo-conversion a efficiency (PCE) now surpassing 22%,[3, 4] compared to a PCE of 3.9% when initially introduced in 2009,[5] metal halide perovskites now compare favorably in the efficiency metric with well-established technologies such as polycrystalline silicon, copper-indium-gallium-selenide, and cadmium-telluride solar cells.

Although the investigation of metal halide perovskites as candidates for the active layer in solar cells started with methylammonium lead iodide ($MAPbI_3$)[5], investigators have recently found that replacing the methylammonium (MA) cation with the formamidinium (FA) cation, or having a mixture of the two, yields higher efficiency and more stable perovskite solar cells.[6, 7] FA-based perovskites have shown superior optoelectronic properties such as extended carrier diffusion lengths and lifetimes when compared to their MA-containing analogues, both in polycrystalline and single-crystal forms.[8-11] On the other hand, mixed halide perovskites (MHPs) have shown an enhanced stability and a bandgap tunability upon engineering the halide (Cl, Br, or I) composition, which makes them ideal for stable and high-efficiency tandem solar cells, light emitting diode (LED) applications, and lasers.[7, 12-14] Traditionally, perovskite materials are synthesized using solvent synthesis (SS) routes, but recently a mechanochemical synthesis (MCS) technique has been proposed as a solvent-free and scalable method to prepare halide perovskite materials. This methodology shows enhanced material properties, achieving better or similar solar cell device performance when compared to SS-prepared devices, along with great flexibility in tuning the dimensionality (3D, 2D, or 0D) of the prepared perovskite materials.[15-20] MCS has been successfully utilized for a long time in other material systems including metal-

organic frameworks (MOFs),[21-23] polymorphs in drug design,[24-26] and composite/metal oxide nanomaterials.[27, 28]

Solid-state nuclear magnetic resonance (NMR) spectroscopy is a highly sensitive tool for identifying atomic-level chemical structure and dynamics. With the ^{207}Pb nucleus exhibiting a large chemical shift range of nearly 20,000 ppm, ^{207}Pb NMR spectroscopy is ideal for the study of the Pb chemical environment.[29-35] Hence, the technique is applied in our investigation of MCS FA-MHPs.

$FAPb(Br_xI_{1-x})_3$, where $0 < x < 1$, has been the focus of research efforts exploring the tunable bandgap and charge carrier dynamics for applications in tandem solar cells and LEDs.[6, 7, 10, 36] In some of these studies it was reported that when $0.3 < x < 0.5$, no crystalline phase can be achieved using traditional solvent synthesis (SS) techniques, but rather an amorphous phase is obtained, which has been attributed to a phase transition from a trigonal ($x < 0.3$) to a cubic ($x > 0.5$) structure. Nevertheless, high-resolution neutron powder diffraction data suggests that α-$FAPbI_3$ ($x = 0$) adopts the cubic (Pm-3m) perovskite unit cell at room temperature[37] rather than the trigonal structure reported for high-temperature solution-deposited α-$FAPbI_3$ films.[38, 39] This is in agreement with observations based on single-crystal or powder X-ray diffraction (pXRD) analyses of α-$FAPbI_3$ prepared by the inverse temperature crystallization (ITC) technique.[40] Aside from $FAPb(Br_xI_{1-x})_3$ MHPs, $FAPbCl_3$ and $FAPb(Cl_xBr_{1-x})_3$ MHPs have rarely been studied; the few studies have focused on nanoparticles.[41-45]

In this work, we explore the MCS route to synthesize FA-based MHPs and probe their long- and short-range chemical structure using pXRD and ^{207}Pb NMR spectroscopy, respectively. In addition, their optical properties are explored using reflectance measurements. We find that

MCS is an effective way to prepare FA-MHP solid-solutions with superior control over halide stoichiometry, including compositions not previously accessible using traditional SS methods. We also compare samples of the same/similar composition (by synthetic loading or final product composition) prepared by SS and MCS.

The $FAPb(Cl_xBr_{1-x})_3$ and $FAPb(Br_xI_{1-x})_3$ MHPs series were prepared by MCS either by hand grinding (HG) or by ball milling (BM) (Scheme 1), starting with their respective parent perovskites, $FAPbX_3$ (see Supporting Information). For each series, three MHPs (x = 0.25, 0.5, 0.75) were synthesized. Figures 1a and 1b show pXRD and ^{207}Pb NMR results for the three parent perovskites and two MHPs, namely, $FAPb(Cl_{0.5}Br_{0.5})_3$ and $FAPb(Br_{0.5}I_{0.5})_3$ (see Figures S1-S6 for complete data set for each series, along with the reflectance measurements). The ^{207}Pb chemical shifts ($\delta_{cs}(^{207}Pb)$) of the parent compounds shift to higher frequency as Cl is replaced by larger and less electronegative halides Br or I, spanning nearly 2,000 ppm ($[PbCl_6]^{4-}$ to $[PbI_6]^{4-}$) as shown in Figures 1b and S7. This observed behavior for $\delta_{cs}(^{207}Pb)$ is similar to what has been previously reported for $MAPbX_3$ and other metal halides.[33, 34, 46, 47] In addition, the ^{207}Pb NMR line widths increase on halide substitution from X = Cl to Br to I, with FWHM values of approximately 4.3, 15 and 22 kHz, respectively at 7.05 T (Table 1). The Pb cations are located at sites of octahedral symmetry ($[PbX_xX'_{6-x}]^{4-}$ units) and thus each ^{207}Pb nucleus is spin-spin coupled (both direct and indirect) to six halide nuclei with nuclear spin I = 3/2 ($^{35/37}$Cl or $^{79/81}$Br) or 5/2 (^{127}I). ^{207}Pb NMR measurements of $MAPbX_3$ compounds when in their cubic phases also yield symmetric broad peaks despite the exclusion of magnetic shielding anisotropy as a line broadening mechanism. Thus, the line broadening in that case was ascribed by the authors[47] to be primarily due to spin-spin coupling interactions and spin-spin relaxation. A similar effect is thought to be at play in the closely related compounds considered here.[30, 34, 48] A Gaussian-like α-

$FAPbI_3$ resonance which does not broaden at higher fields (Figure S8) is observed; in contrast, an asymmetric ^{207}Pb NMR powder pattern that increases in breadth with field strength is observed for the non-perovskite δ-$FAPbI_3$ (Figure S9 and S10 (pXRD)), indicating that δ-$FAPbI_3$ has a sizable magnetic shielding anisotropy. Fitting the spectra acquired at 11.75 T yields isotropic chemical shift, δ_{iso} of 1150 ppm, a span (Ω) of 620 ppm and skew (κ) of 0.65; we note that the δ_{cs} for δ-$FAPbI_3$ shifts to lower frequency compared to that for α-$FAPbI_3$ (Table 1 and Figure S11).

Pure cubic phases are confirmed through pXRD for all MHPs prepared via MCS and a Gaussian-like distribution of ^{207}Pb NMR resonances is observed, consistent with distinct local $[PbX_xX'_{6-x}]^{4-}$ chemical environments. ^{207}Pb NMR spectra at different fields for the HG $FAPb(Cl_{0.5}Br_{0.5})_3$ mixture are shown in Figure S12, revealing five resolved resonances that are assigned to $[PbBr_6]^{4-}$, $[PbCl_1Br_5]^{4-}$/$[PbCl_2Br_4]^{4-}$, $[PbCl_3Br_3]^{4-}$, $[PbCl_4Br_2]^{4-}$/$[PbCl_5Br_1]^{4-}$ and $[PbCl_6]^{4-}$; the assignment and fitting of experimental data acquired at 11.75 and 21.1 T are consistent with a binomial-like distribution for random Cl/Br mixing, as shown in Figure S13b. Other mixtures in the series considered here also display binomial-like distributions based on their corresponding stoichiometric compositions, see Figure S13. To assess the homogeneity of the halide ions about the Pb environment in these solid solutions, a series of ^{207}Pb 2D EXSY NMR spectra (Figure 1c) were obtained for the hand ground $FAPb(Cl_{0.5}Br_{0.5})_3$ sample with mixing times varying between 10 and 2,000 μs. Recently we showed that this method provides atomic-level insight into the arrangement of the halide ions for a series of MA-containing $[PbX_xX'_{6-x}]^{4-}$ species.[49] The EXSY spectra indicated fast exchange between various $[PbX_xX'_{6-x}]^{4-}$ units, and thus we concluded that the MHP consisted of a solid solution rather than either phase-separated materials or micro/nano domains, for which fast exchange would not be

observed. In a similar manner, the HG-FAPb($Cl_{0.5}Br_{0.5}$)$_3$ sample clearly displays exchange for the individual Pb environments (e.g., $[PbCl_1Br_5]^{4-}$, $[PbCl_2Br_4]^{4-}$, $[PbCl_3Br_3]^{4-}$, $[PbCl_4Br_2]^{4-}$ and $[PbCl_5Br_1]^{4-}$) with longer mixing times leading to the formation of cross peaks to neighbors and next-nearest neighbors. Hence, as seen in the sister MA mixed Cl/Br perovskites, Cl/Br-based FA-MHPs display homogeneously mixed solid solutions absent of phase separation when mechanically mixed for sufficient time.

Pb-207 NMR spectra for the BM-FAPb($Br_{0.5}I_{0.5}$)$_3$ sample acquired at 11.75 or 21.1 T were not resolved because of the line broadening attributed to ^{207}Pb-$^{79/81}$Br ^{207}Pb-^{127}I spin-spin interactions, spin-spin relaxation, and local disorder imparted by the high-energy BM process.[49] Higher magnetic field strengths may improve the resolution and line shape assessment (i.e., contribution from chemical shift anisotropy) as only slight evidence of multiple resonances begin to emerge at 21.1 T (Figure S14).[50] The resonances for the I- and Br-rich MHPs lie between those for their respective parent perovskites and the 50/50 mixture (Figures S4 and S15), suggesting a statistical distribution of $[PbX_xX_{6-x}]^{4-}$ populations. Thus, behavior similar to that observed for the HG Br/Cl MHP series is suggested, although in this case it was not possible to resolve individual sites.

Tracking the lattice constants and optical bandbaps (extracted from pXRD and Tauc plots, respectively)[51] within these series of MCS-MHPs (Figures 1d & 1e) demonstrates a linear evolution with halide substitution from pure $FAPbCl_3$ to α-$FAPbI_3$, agreeing with Vegard's law.[52, 53] The NMR spectroscopy and pXRD results (Figure 1) together indicate that a MCS route leads to homogeneous atomic-level solid-solutions of FA-MHPs.

HG-MCS of $FAPbCl_3$ and $FAPbBr_3$ samples was sufficient to synthesize single pure phases of $FAPb(Cl_xBr_{1-x})_3$ solid solutions, but for $FAPb(Br_xI_{1-x})_3$ series, further treatment was required. A high temperature (200 ˚C – 1 hr) annealing step was used to obtain the Br-rich (i.e., $FAPb(Br_{0.75}I_{0.25})_3$) composition (see Figure S16 for pXRD and ^{207}Pb NMR data taken at various steps of the HG process). This approach was unsuccessful for $FAPb(Br_{0.50}I_{0.50})_3$ and $FAPb(Br_{0.25}I_{0.75})_3$ and led to rapid decomposition of the materials or impure MHP products, or both (see Figure S17). This is thought to be partially due to the decomposition of $FAPbI_3$ under thermal annealing[39] before a single MHP phase is formed, since pXRD indicates that PbI_2 was formed during the annealing process to form 50/50 Br/I or I-rich FA-MHPs. To avoid possible degradation/decomposition and to achieve single pure phases for $FAPb(Br_{0.50}I_{0.50})_3$ and $FAPb(Br_{0.25}I_{0.75})_3$ MHP solid solutions, a high-energy MCS method adopting BM was implemented (see Figures 1a and S2). The BM method provides sufficient mechanical energy to form these phases within 30-60 minutes, at sample temperatures of approximately +50 ^{o}C, similar to that applied in other systems;[54] a detailed discussion of possible mechanisms of crystal formation through BM-MCS can be found elsewhere.[19, 55-57] The success of BM near room temperature is mostly due to the high halide ion mobility in lead halide perovskite systems.[58-60] It has been shown previously that a solid-state synthesis method starting from parent compounds can be used to prepare a stoichiometric $MAPb(Br_{0.50}I_{0.50})_3$, but only after a heating protocol is applied, with partial sample decomposition observed at temperatures > 250 ˚C.[34] The BM method described here may provide a versatile and highly adaptable approach for other hybrid perovskites, overcoming the need for any high-temperature treatments.[16]

Figure 2 illustrates a comparison of pXRD, ^{207}Pb NMR and reflectance data for $FAPb(Cl_{0.25}Br_{0.75})_3$ prepared using the MCS approach with those prepared using the SS method

(see SI for experimental details). Both techniques yield nearly identical experimental results, with SS showing a slightly blue-shifted reflection edge. This observed shift is due to more Cl content (confirmed by EDX) versus the stoichiometric HG composition. Even though the synthetic loading for both samples is Br - 75 % and Cl - 25%, the HG compound has an atomic % of Br/Cl of 3.06/1, while the SS compound is 2.4/1, demonstrating that fine control over composition is possible through MCS. The ^{207}Pb NMR spectra for both samples are similar, but the MCS approach provides spectra with higher resolution between different Pb coordination environments. In addition, the resonance centered at δ_{cs} ~ 100 ppm (Figure 2c) is higher in intensity for the SS (vs MCS) sample corresponding to the higher Cl concentration, as confirmed by EDX.

Attempts to prepare a stoichiometric $FAPb(Br_{0.5}I_{0.5})_3$ using the SS route[34] as described for $MAPb(Br_{0.5}I_{0.5})_3$ were unsuccessful; pXRD and ^{207}Pb NMR data suggest that a Br-rich final product was obtained (Figure 3). Due to the distinct thermodynamic and kinetic characteristic in forming MHPs through solvent synthesis vs. MCS, the $FAPb(Br_{0.5}I_{0.5})_3$ mixture was only achieved using the latter (Figure 1), while the SS habitually led to a Br-rich phase.[34] In other words, preparing $FAPb(Br_{0.50}I_{0.50})_3$ by SS led to a product similar to the MCS of $FAPb(Br_{0.75}I_{0.25})_3$, as shown in Figure 3. Hence, the BM-MCS approach described above was developed to prepare these MHPs.

A systematic shift of the δ_{cs} occurs as the Pb environment arranges halides about its six-coordinate center as Br replaces Cl (Figure 2 & S3) or as I replaces Br (Figure S4). Previously, we illustrated that DFT calculations using $[PbX_xX'_{6-x}]^{4-}$ anion models can assist in unambiguously assigning unique Pb environments.[49] Figure 3c shows the results obtained using ADF to calculate the unique δ_{cs} of $[PbBr_xI_{6-x}]^{4-}$ revealing a similar change as Br is replaced with

I. Accordingly the experimental and DFT results indicate up to four local Pb polyhedra are contributing to the line shape in a binomial-like distribution (Figures S19 and S20) which include $[PbBr_6]^{4-}$, $[PbBr_5I]^{4-}$, $[PbBr_4I_2]^{4-}$-*cis, trans* and $[PbBr_3I_3]^{4-}$-*fac, mer*. For completeness, a series of ^{1}H and ^{13}C MAS NMR spectra were acquired on the parent perovskites series (see Supporting Information, Figures S21-S23).

We have presented a MCS approach for preparing FA-MHPs with fine control over halide compositions, including some not accessible by the traditional SS method. All MCS MHPs show a solid-solution behavior, with both crystal lattice constants and optical bandgaps conforming to Vegard's law. Probing local Pb environments of the $[PbX_XX'_{6-X}]^{4-}$ octahedra in MHPs through ^{207}Pb NMR spectroscopy, distinct Pb chemical structures are identified, and their estimated populations adopt a binomial-like distribution, as expected for solid-solutions. The 2D EXSY NMR experiment confirms that the MCS method provides a homogeneously mixed halide perovskite solid-solution at the atomic scale for $FAPb(Cl_xBr_{1-x})_3$. Comparing SS results to MCS for samples with similar final compositions, comparable structural and physical properties are determined; however, efficient control of stoichiometric synthesis for the MHPs studied here is better with the MCS method. As recently reported for single halide perovskites prepared using a MCS approach, these materials lead to an improvement in device performance when compared to SS counterparts.[15-19] Hence, we hypothesize that the excellent compositional regulation in preparing FA-containing MHPs via MCS methods could provide superior control in optoelectronic properties leading to improved control in fabrication approaches. This work paves the way to further understanding the underlying complex physical property behavior by providing atomic-level insight into these MHP solid-solutions, targeting the development of highly efficient and stable devices. As perovskite materials continue to evolve for photovoltaic

applications careful characterization is essential. This study illustrates the importance of combining long-range diffraction based methods as well as probing the atomic-scale using 1D and 2D NMR spectroscopy as key components to unravel these intrinsically complex materials.

ACKNOWLEDGMENTS

The Natural Sciences and Engineering Research Council (NSERC) of Canada and the University of Alberta are acknowledged for generous research support (V.K.M.). A.M.A. acknowledges scholarship support from Alberta Innovates Technology Futures (AITF). M.H. is partially supported by the Government of Alberta Queen Elizabeth II Graduate Scholarship. K.S. acknowledges direct and indirect (equipment) funding support from NRC- NINT and CFI. The authors recognize continued generous funding from the NSERC CREATE and Deutsche Forschungsgemeinschaft DFG (IRTG2022) for Alberta/Technical University of Munich International Graduate School for Hybrid Functional Materials (ATUMS). Access to the 21.1 T NMR spectrometer was provided by the National Ultrahigh-Field NMR Facility for Solids (Ottawa, Canada), a national research facility funded by a consortium of Canadian Universities and by an NSERC RTI grant, and supported by the National Research Council of Canada and Bruker BioSpin, and managed by the University of Ottawa (http://nmr900.ca).

SUPPORTING INFORMATION

Materials and methods, powder XRD, solid-state NMR spectroscopy, quantum chemical calculations and optical bandgap measurement details are available in the Supporting Information.

AUTHOR INFORMATION

*Corresponding Author: vladimir.michaelis@ualberta.ca

[§]Author Contributions: AMA and AK contributed equally to this work.

The authors declare no competing financial interests.

REFERENCES

1. Adinolfi, V.; Peng, W.; Walters, G.; Bakr, O. M.; Sargent, E. H., The Electrical and Optical Properties of Organometal Halide Perovskites Relevant to Optoelectronic Performance. *Adv. Mater.* **2017,** *30*, 1700764.

2. Zhao, Y.; Zhu, K., Solution Chemistry Engineering Toward High-Efficiency Perovskite Solar Cells. *J. Phys. Chem. Lett.* **2014,** *5* (23), 4175-4186.

3. Yang, W. S.; Park, B.-W.; Jung, E. H.; Jeon, N. J.; Kim, Y. C.; Lee, D. U.; Shin, S. S.; Seo, J.; Kim, E. K.; Noh, J. H.*, et al.*, Iodide Management in Formamidinium-Lead-Halide–Based Perovskite Layers for Efficient Solar Cells. *Science* **2017,** *356* (6345), 1376-1379.

4. Shin, S. S.; Yeom, E. J.; Yang, W. S.; Hur, S.; Kim, M. G.; Im, J.; Seo, J.; Noh, J. H.; Seok, S. I., Colloidally Prepared La-Doped $BaSnO_3$ Electrodes for Efficient, Photostable Perovskite Solar Cells. *Science* **2017,** *356*, 167-171.

5. Kojima, A.; Teshima, K.; Shirai, Y.; Miyasaka, T., Organometal Halide Perovskites as Visible-Light Sensitizers for Photovoltaic Cells. *J. Am. Chem. Soc.* **2009,** *131* (17), 6050-6051.

6. Eperon, G. E.; Stranks, S. D.; Menelaou, C.; Johnston, M. B.; Herz, L. M.; Snaith, H. J., Formamidinium Lead Trihalide: A Broadly Tunable Perovskite for Efficient Planar Heterojunction Solar Cells. *Energy Environ. Science* **2014,** *7* (3), 982-988.

7. Eperon, G. E.; Leijtens, T.; Bush, K. A.; Prasanna, R.; Green, T.; Wang, J. T.-W.; McMeekin, D. P.; Volonakis, G.; Milot, R. L.; May, R.*, et al.*, Perovskite-Perovskite Tandem Photovoltaics with Optimized Bandgaps. *Science* **2016,** *354*, 861-865.

8. Hanusch, F. C.; Wiesenmayer, E.; Mankel, E.; Binek, A.; Angloher, P.; Fraunhofer, C.; Giesbrecht, N.; Feckl, J. M.; Jaegermann, W.; Johrendt, D.*, et al.*, Efficient Planar Heterojunction Perovskite Solar Cells Based on Formamidinium Lead Bromide. *J. Phys. Chem. Lett.* **2014,** *5* (16), 2791-2795.

9. Pellet, N.; Gao, P.; Gregori, G.; Yang, T.-Y.; Nazeeruddin, M. K.; Maier, J.; Grätzel, M., Mixed-Organic-Cation Perovskite Photovoltaics for Enhanced Solar-Light Harvesting. *Angew. Chem. Int. Ed.* **2014,** *53* (12), 3151-3157.

10. Rehman, W.; Milot, R. L.; Eperon, G. E.; Wehrenfennig, C.; Boland, J. L.; Snaith, H. J.; Johnston, M. B.; Herz, L. M., Charge-Carrier Dynamics and Mobilities in Formamidinium Lead Mixed-Halide Perovskites. *Adv. Mater.* **2015,** *27* (48), 7938-7944.

11. Zhumekenov, A. A.; Saidaminov, M. I.; Haque, M. A.; Alarousu, E.; Sarmah, S. P.; Murali, B.; Dursun, I.; Miao, X.-H.; Abdelhady, A. L.; Wu, T.*, et al.*, Formamidinium Lead Halide Perovskite Crystals with Unprecedented Long Carrier Dynamics and Diffusion Length. *ACS Energy Letters* **2016,** *1* (1), 32-37.

12. Levchuk, I.; Osvet, A.; Tang, X.; Brandl, M.; Perea, J. D.; Hoegl, F.; Matt, G. J.; Hock, R.; Batentschuk, M.; Brabec, C. J., Brightly Luminescent and Color-Tunable Formamidinium Lead Halide Perovskite $FAPbX_3$ (X = Cl, Br, I) Colloidal Nanocrystals. *Nano Lett.* **2017,** *17* (5), 2765-2770.

13. Tan, H.; Jain, A.; Voznyy, O.; Lan, X.; García de Arquer, F. P.; Fan, J. Z.; Quintero-Bermudez, R.; Yuan, M.; Zhang, B.; Zhao, Y.*, et al.*, Efficient and Stable Solution-Processed Planar Perovskite Solar Cells via Contact Passivation. *Science* **2017,** *355*, 722-726.

14. Wang, C.; Zhang, Y.; Wang, A.; Wang, Q.; Tang, H.; Shen, W.; Li, Z.; Deng, Z., Controlled Synthesis of Composition Tunable Formamidinium Cesium Double Cation Lead Halide Perovskite Nanowires and Nanosheets with Improved Stability. *Chem. Mater.* **2017,** *29* (5), 2157-2166.

15. Prochowicz, D.; Franckevicius, M.; Cieslak, A. M.; Zakeeruddin, S. M.; Gratzel, M.; Lewinski, J., Mechanosynthesis of the Hybrid Perovskite $CH_3NH_3PbI_3$: Characterization and the Corresponding Solar Cell Efficiency. *J. Mater. Chem. A* **2015,** *3* (41), 20772-20777.

16. Prochowicz, D.; Yadav, P.; Saliba, M.; Saski, M.; Zakeeruddin, S. M.; Lewiński, J.; Grätzel, M., Mechanosynthesis of Pure Phase Mixed-Cation $MA_XFA_{1-X}PbI_3$ Hybrid Perovskites: Photovoltaic Performance and Electrochemical Properties. *Sustain. Energy Fuels* **2017,** *1* (4), 689-693.

17. Elseman, A. M.; Rashad, M. M.; Hassan, A. M., Easily Attainable, Efficient Solar Cell with Mass Yield of Nanorod Single-Crystalline Organo-Metal Halide Perovskite Based on a Ball Milling Technique. *ACS Sustain. Chem. Eng.* **2016,** *4* (9), 4875-4886.

18. Jana, A.; Mittal, M.; Singla, A.; Sapra, S.; Grätzel, M.; Lewiński, J.; Tong, Y.; Polavarapu, L.; Feldmann, J.; Urban, A. S.*, et al.*, Solvent-Free, Mechanochemical Syntheses of Bulk Trihalide Perovskites and Their Nanoparticles. *Chem. Commun.* **2017,** *53* (21), 3046-3049.

19. Zhu, Z.-Y.; Yang, Q.-Q.; Gao, L.-F.; Zhang, L.; Shi, A.-Y.; Sun, C.-L.; Wang, Q.; Zhang, H.-L., Solvent-Free Mechanosynthesis of Composition-Tunable Cesium Lead Halide Perovskite Quantum Dots. *J. Phys. Chem. Lett.* **2017,** *8* (7), 1610-1614.

20. Pal, P.; Saha, S.; Banik, A.; Sarkar, A.; Biswas, K., All-Solid-State Mechanochemical Synthesis and Post-Synthetic Transformation of Inorganic Perovskite-Type Halides. *Chem. Eur. J.* **2018,** *24* (8), 1811-1815.

21. Klimakow, M.; Klobes, P.; Thünemann, A. F.; Rademann, K.; Emmerling, F., Mechanochemical Synthesis of Metal−Organic Frameworks: A Fast and Facile Approach Toward Quantitative Yields and High Specific Surface Areas. *Chem. Mater.* **2010,** *22* (18), 5216-5221.

22. Friščić, T., Metal-Organic Frameworks: Mechanochemical Synthesis Strategies. In *Encyclopedia of Inorganic and Bioinorganic Chemistry*, John Wiley & Sons, Ltd: 2011.

23. Singh, N. K.; Hardi, M.; Balema, V. P., Mechanochemical Synthesis of an Yttrium Based Metal-Organic Framework. *Chem. Commun.* **2013,** *49* (10), 972-974.

24. Zhou, Y.; Guo, F.; Hughes, C. E.; Browne, D. L.; Peskett, T. R.; Harris, K. D. M., Discovery of New Metastable Polymorphs in a Family of Urea Co-Crystals by Solid-State Mechanochemistry. *Cryst. Growth Des.* **2015,** *15* (6), 2901-2907.

25. Hasa, D.; Miniussi, E.; Jones, W., Mechanochemical Synthesis of Multicomponent Crystals: One Liquid for One Polymorph? A Myth to Dispel. *Cryst. Growth Des.* **2016,** *16* (8), 4582-4588.

26. Fischer, F.; Heidrich, A.; Greiser, S.; Benemann, S.; Rademann, K.; Emmerling, F., Polymorphism of Mechanochemically Synthesized Cocrystals: A Case Study. *Cryst. Growth Des.* **2016,** *16* (3), 1701-1707.

27. Xu, C.; De, S.; Balu, A. M.; Ojeda, M.; Luque, R., Mechanochemical Synthesis of Advanced Nanomaterials for Catalytic Applications. *Chem. Commun.* **2015,** *51* (31), 6698-6713.

28. Wu, H.; Li, Q., Application of Mechanochemical Synthesis of Advanced Materials. *J. Adv. Ceram.* **2012,** *1* (2), 130-137.

29. Dybowski, C.; Smith, M. L.; Hepp, M. A.; Gaffney, E. J.; Neue, G.; Perry, D. L., ^{207}Pb NMR Chemical-Shift Tensors of the Lead (II) Halides and the Lead (II) Hydroxyhalides. *Appl. Spectrosc.* **1998,** *52* (3), 426-429.

30. Askar, A. M.; Bernard, G. M.; Wiltshire, B.; Shankar, K.; Michaelis, V. K., Multinuclear Magnetic Resonance Tracking of Hydro, Thermal, and Hydrothermal Decomposition of $CH_3NH_3PbI_3$. *J. Phys. Chem. C* **2017,** *121* (2), 1013-1024.

31. Wrackmeyer, B., Application of ^{207}Pb NMR Parameters. In *Annual Reports on NMR Spectroscopy*, Academic Press: 2002; Vol. Volume 47, pp 1-37.

32. Aliev, A. E.; Law, R. V., Chapter 7 Solid State NMR Spectroscopy. In *Nuclear Magnetic Resonance: Volume 43*, The Royal Society of Chemistry: 2014; Vol. 43, pp 286-344.

33. Rosales, B. A.; Hanrahan, M. P.; Boote, B. W.; Rossini, A. J.; Smith, E. A.; Vela, J., Lead Halide Perovskites: Challenges and Opportunities in Advanced Synthesis and Spectroscopy. *ACS Energy Lett.* **2017,** *2* (4), 906-914.

34. Rosales, B. A.; Men, L.; Cady, S. D.; Hanrahan, M. P.; Rossini, A. J.; Vela, J., Persistent Dopants and Phase Segregation in Organolead Mixed-Halide Perovskites. *Chem. Mater.* **2016,** *28* (19), 6848-6859.

35. Lignos, I.; Protesescu, L.; Emiroglu, D. B.; Maceiczyk, R.; Schneider, S.; Kovalenko, M. V.; deMello, A. J., Unveiling the Shape Evolution and Halide-Ion-Segregation in Blue-Emitting Formamidinium Lead Halide Perovskite Nanocrystals Using an Automated Microfluidic Platform. *Nano Lett.* **2018,** *18*, 1246-1252.

36. McMeekin, D. P.; Sadoughi, G.; Rehman, W.; Eperon, G. E.; Saliba, M.; Hörantner, M. T.; Haghighirad, A.; Sakai, N.; Korte, L.; Rech, B.*, et al.*, A Mixed-Cation Lead Mixed-Halide Perovskite Absorber for Tandem Solar Cells. *Science* **2016,** *351* (6269), 151-155.

37. Weller, M. T.; Weber, O. J.; Frost, J. M.; Walsh, A., Cubic Perovskite Structure of Black Formamidinium Lead Iodide, α-$[HC(NH_2)_2]PbI_3$, at 298 K. *J. Phys. Chem. Lett.* **2015,** *6* (16), 3209-3212.

38. Binek, A.; Hanusch, F. C.; Docampo, P.; Bein, T., Stabilization of the Trigonal High-Temperature Phase of Formamidinium Lead Iodide. *J. Phys. Chem. Lett.* **2015,** *6* (7), 1249-1253.

39. Pool, V. L.; Dou, B.; Van Campen, D. G.; Klein-Stockert, T. R.; Barnes, F. S.; Shaheen, S. E.; Ahmad, M. I.; van Hest, M. F. A. M.; Toney, M. F., Thermal Engineering of $FAPbI_3$ Perovskite Material via Radiative Thermal Annealing and in situ XRD. *Nature Comm.* **2017,** *8*, 14075.

40. Saidaminov, M. I.; Abdelhady, A. L.; Maculan, G.; Bakr, O. M., Retrograde Solubility of Formamidinium and Methylammonium Lead Halide Perovskites Enabling Rapid Single Crystal Growth. *Chem. Commun.* **2015,** *51* (100), 17658-17661.

41. Jang, D. M.; Kim, D. H.; Park, K.; Park, J.; Lee, J. W.; Song, J. K., Ultrasound Synthesis of Lead Halide Perovskite Nanocrystals. *J. Mater. Chem. C* **2016,** *4* (45), 10625-10629.

42. Weidman, M. C.; Seitz, M.; Stranks, S. D.; Tisdale, W. A., Highly Tunable Colloidal Perovskite Nanoplatelets through Variable Cation, Metal, and Halide Composition. *ACS Nano* **2016,** *10* (8), 7830-7839.

43. Wang, J.; Peng, J.; Sun, Y.; Liu, X.; Chen, Y.; Liang, Z., $FAPbCl_3$ Perovskite as Alternative Interfacial Layer for Highly Efficient and Stable Polymer Solar Cells. *Advanced Electronic Materials* **2016,** *2* (11), 1600329.

44. Hills-Kimball, K.; Nagaoka, Y.; Cao, C.; Chaykovsky, E.; Chen, O., Synthesis of Formamidinium Lead Halide Perovskite Nanocrystals through Solid-Liquid-Solid Cation Exchange. *J. Mater. Chem. C* **2017,** *5* (23), 5680-5684.

45. Minh, D. N.; Kim, J.; Hyon, J.; Sim, J. H.; Sowlih, H. H.; Seo, C.; Nam, J.; Eom, S.; Suk, S.; Lee, S.*, et al.*, Room-Temperature Synthesis of Widely Tunable Formamidinium Lead Halide Perovskite Nanocrystals. *Chem. Mater.* **2017,** *29* (13), 5713-5719.

46. Roiland, C.; Trippe-Allard, G.; Jemli, K.; Alonso, B.; Ameline, J.-C.; Gautier, R.; Bataille, T.; Le Polles, L.; Deleporte, E.; Even, J.*, et al.*, Multinuclear NMR as a Tool for Studying Local Order and Dynamics in $CH_3NH_3PbX_3$ (X = Cl, Br, I) Hybrid Perovskites. *Phys. Chem. Chem. Phys.* **2016,** *18* (39), 27133-27142.

47. Bernard, G. M.; Wasylishen, R. E.; Ratcliffe, C. I.; Terskikh, V.; Wu, Q.; Buriak, J. M.; Hauger, T., Methylammonium Cation Dynamics in Methylammonium Lead Halide Perovskites: A Solid-State NMR Perspective. *J. Phys. Chem. A* **2018,** *122*, 1560-1573.

48. Senocrate, A.; Moudrakovski, I.; Kim, G. Y.; Yang, T.-Y.; Gregori, G.; Grätzel, M.; Maier, J., The Nature of Ion Conduction in Methylammonium Lead Iodide: A Multimethod Approach. *Angew. Chem. Int. Ed.* **2017,** *56* (27), 7755-7759.

49. Karmakar, A.; Askar, A. M.; Bernard, G. M.; Terskikh, V. V.; Ha, M.; Patel, S.; Shankar, K.; Michaelis, V. K., Mechanochemical Synthesis of Methylammonium Lead Mixed–Halide Perovskites: Unraveling the Solid-Solution Behavior Using Solid-State NMR. *Chem. Mater.* **2018,** *30* (7), 2309-2321.

50. Keeler, E. G.; Michaelis, V. K.; Colvin, M. T.; Hung, I.; Gor'kov, P. L.; Cross, T. A.; Gan, Z.; Griffin, R. G., ^{17}O MAS NMR Correlation Spectroscopy at High Magnetic Fields. *J. Am. Chem. Soc.* **2017,** *139* (49), 17953-17963.

51. Xia, Z.; Zhang, Y.; Molokeev, M. S.; Atuchin, V. V., Structural and Luminescence Properties of Yellow-Emitting $NaScSi_2O_6:Eu^{2+}$ Phosphors: Eu^{2+} Site Preference Analysis and Generation of Red Emission by Codoping Mn^{2+} for White-Light-Emitting Diode Applications. *J. Phys. Chem. C* **2013,** *117* (40), 20847-20854.

52. Vegard, L., Die Konstitution Der Mischkristalle Und Die Raumfüllung Der Atome. *Z. Phys.* **1921,** *5* (1), 17-26.

53. Denton, A. R.; Ashcroft, N. W., Vegard's Law. *Phys. Rev. A* **1991,** *43* (6), 3161-3164.

54. Gupta, S.; Hlova, I. Z.; Kobayashi, T.; Denys, R. V.; Chen, F.; Zavaliy, I. Y.; Pruski, M.; Pecharsky, V. K., Facile Synthesis and Regeneration of $Mg(BH_4)_2$ by High Energy Reactive Ball Milling of MgB_2. *Chem. Commun.* **2013,** *49* (8), 828-830.

55. Friščić, T.; Halasz, I.; Beldon, P. J.; Belenguer, A. M.; Adams, F.; Kimber, S. A. J.; Honkimäki, V.; Dinnebier, R. E., Real-Time and in situ Monitoring of Mechanochemical Milling Reactions. *Nature Chem.* **2012,** *5*, 66-73.

56. Do, J.-L.; Friščić, T., Mechanochemistry: A Force of Synthesis. *ACS Cent. Sci.* **2017,** *3* (1), 13-19.

57. Kaupp, G., Solid-State Molecular Syntheses: Complete Reactions without Auxiliaries Based on the New Solid-State Mechanism. *CrystEngComm* **2003,** *5* (23), 117-133.

58. Yoon, S. J.; Kuno, M.; Kamat, P. V., Shift Happens. How Halide Ion Defects Influence Photoinduced Segregation in Mixed Halide Perovskites. *ACS Energy Lett.* **2017,** *2* (7), 1507-1514.

59. Yoon, S. J.; Draguta, S.; Manser, J. S.; Sharia, O.; Schneider, W. F.; Kuno, M.; Kamat, P. V., Tracking Iodide and Bromide Ion Segregation in Mixed Halide Lead Perovskites During Photoirradiation. *ACS Energy Lett.* **2016,** *1* (1), 290-296.

60. Samu, G. F.; Janáky, C.; Kamat, P. V., A Victim of Halide Ion Segregation. How Light Soaking Affects Solar Cell Performance of Mixed Halide Lead Perovskites. *ACS Energy Lett.* **2017,** *2* (8), 1860-1861.

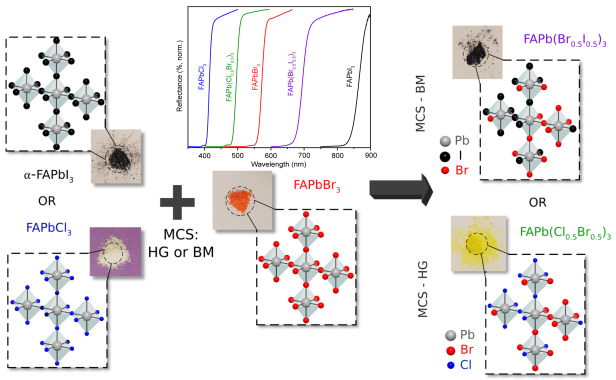

Scheme 1. *MCS preparation of FA-MHPs along with crystal structure diagram highlighting the* $[PbX_xX'_{6-x}]^{4-}$ *octahedral configurations and the normalized reflectance spectra for the parent* $FAPbX_3$ *and the MHPs (HG-*$FAPb(Cl_{0.5}Br_{0.5})_3$*, and BM-*$FAPb(Br_{0.5}I_{0.5})_3$*).*

Table 1. *^{207}Pb NMR Parameters for* $FAPbX_3$ *parent compounds (non-spinning,* B_o*=7.05 T).*

Sample	δ_{cs} (^{207}Pb/ppm)	FWHM/ kHz	T_1/s
$FAPbCl_3$	−454(2)	~4.3	1.53(2)
$FAPbBr_3$	510(7)	~15	1.85(2)
α-$FAPbI_3$	1495(20)	~22	1.94(15)
δ-$FAPbI_3$[a]	1150(15)[b]	-[c]	1.88(20)

a- B_o=11.75 T; b- Isotropic chemical shift, δ_{iso}; c- span, Ω = 620 (30) ppm and skew, κ = 0.65 (5).

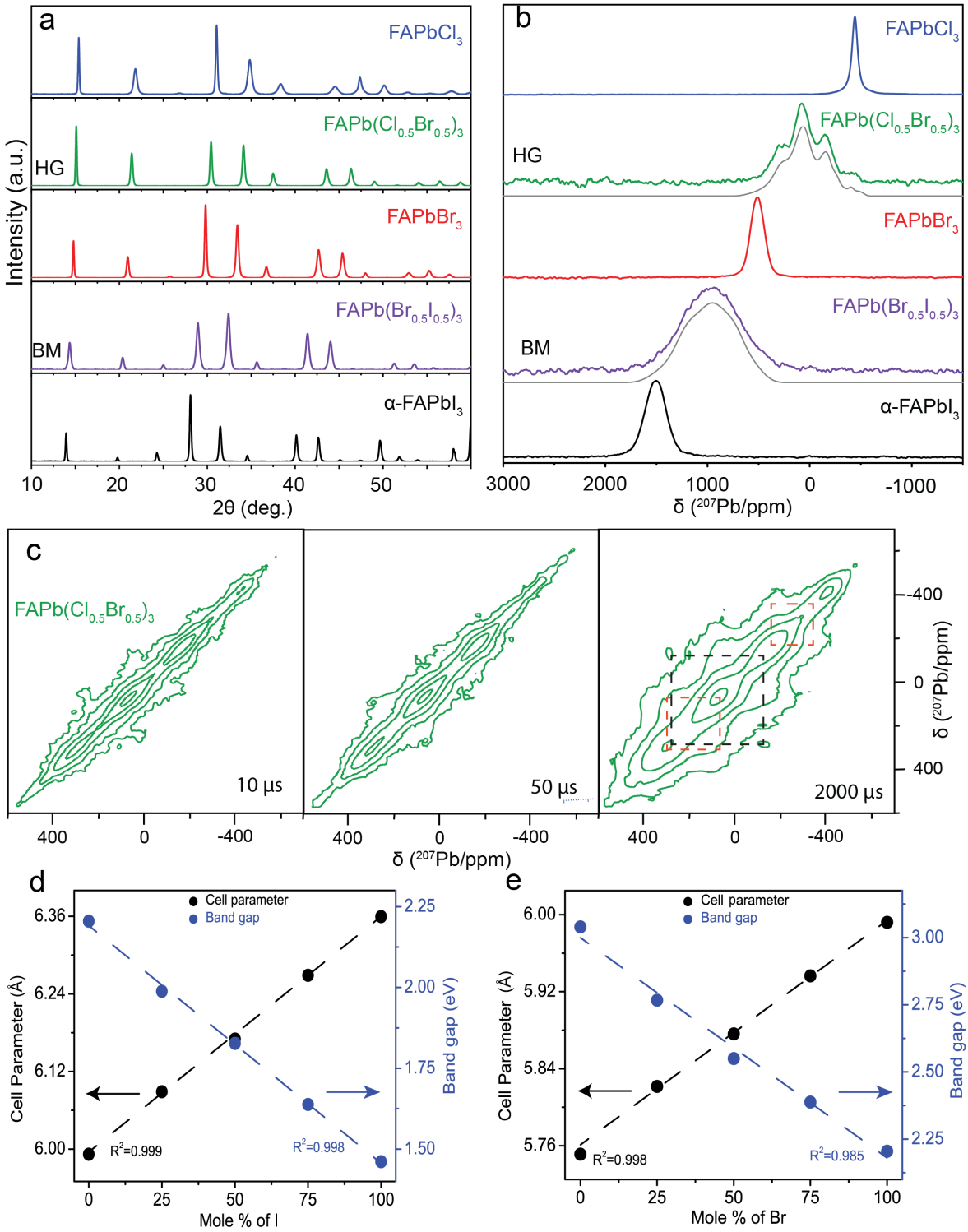

Figure 1. *Powder XRD (a) and non-spinning ^{207}Pb NMR spectra (b, 11.75 T) structural characterization of parent ($FAPbX_3$) and mixed (HG-$FAPb(Cl_{0.5}Br_{0.5})_3$ and BM-$FAPb(Br_{0.5}I_{0.5})_3$) perovskites (simulated spectra in grey). Two-dimensional ^{207}Pb EXSY NMR spectra of HG-$FAPb(Cl_{0.5}Br_{0.5})_3$ (spectra were acquired at 21.1 T under non-spinning conditions at ambient temperature) obtained using 10 (left), 50 (middle) or 2,000 μs (right) mixing times (c). Unit cell and bandgap (extracted from Tauc plots) properties follow a linear regression obeying Vegard's law (cell constants determined from XRD) with halide substitution for the BM-$FAPb(Br_{1-x}I_x)_3$ series (d) and HG-$FAPb(Cl_{1-x}Br_x)_3$ series (e).*

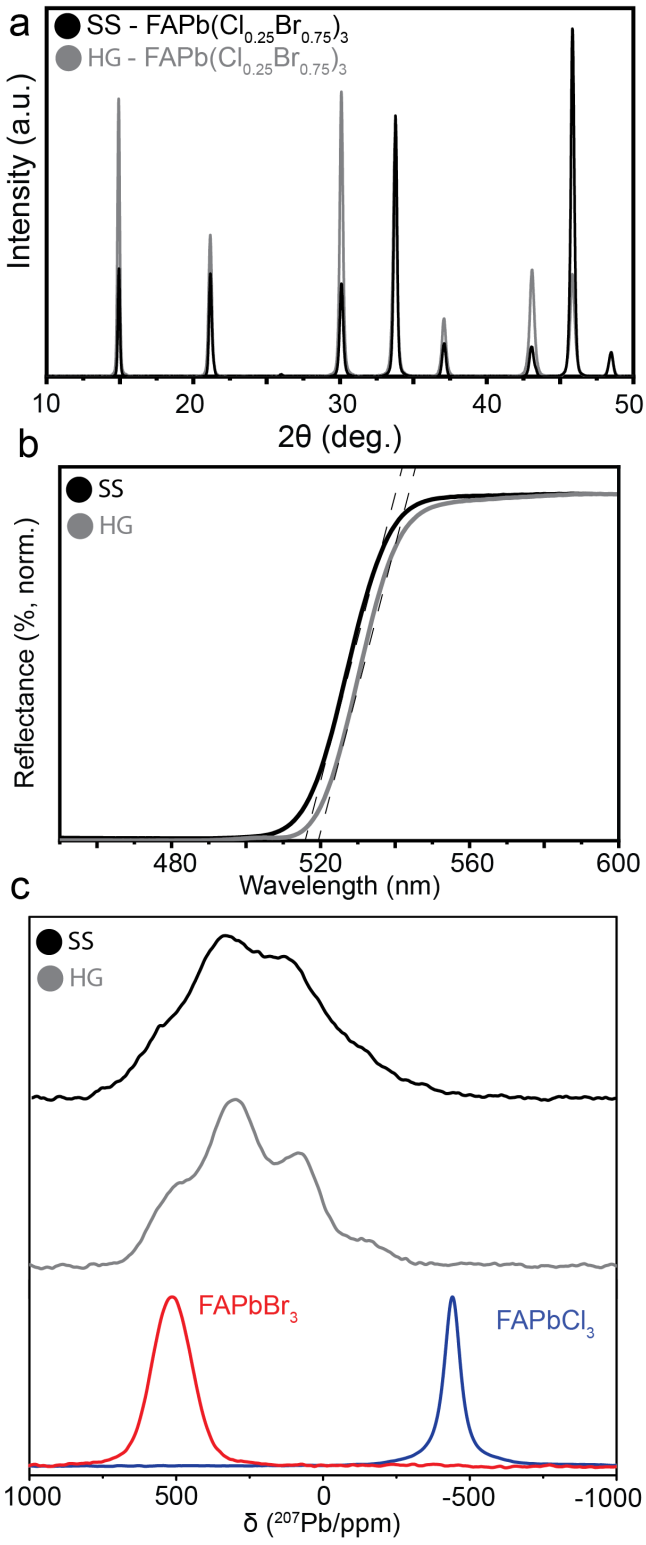

Figure 2. *Structural characterization of $FAPb(Cl_{0.25}Br_{0.75})_3$ prepared by HG or SS approaches using pXRD (a), reflectance (b) and non-spinning ^{207}Pb NMR spectroscopy (c). NMR spectra were acquired at 11.75 T; the corresponding for $FAPbCl_3$ and $FAPbBr_3$ are included for comparison.*

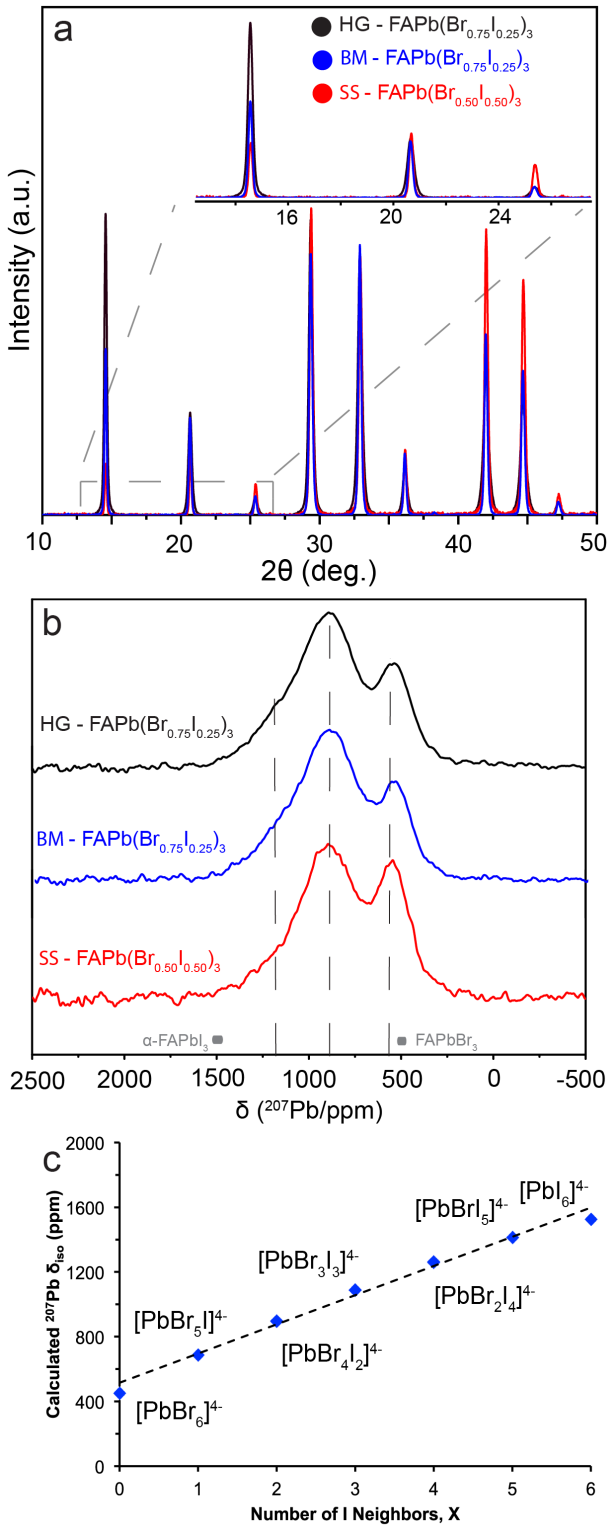

Figure 3. *Comparison of the characteristics for HG-FAPb($Br_{0.75}I_{0.25}$)$_3$ (HG+1h anneal), BM-FAPb($Br_{0.75}I_{0.25}$)$_3$ and SS attempt of FAPb($Br_{0.5}I_{0.5}$)$_3$ (by synthetic loading, see text). (a) pXRD pattern, (b)non-spinning ^{207}Pb NMR spectra (11.75 T) and (c) DFT model anion $[PbBr_xI_{6-x}]^{4-}$ calculations (R^2 = 0.99; y = 180.4x + 515.3).*